J Ther Eng, Vol. 12, No. 1, pp. 1−20, January, 2026

Journal of Thermal Engineering
Web page info: https://jten.yildiz.edu.tr
DOI: 10.14744/thermal.0001073

Research Article

Exergy, energy, exergoenvironmental assessment of a novel combined helium Brayton cycle and transcritical CO_2 cycle for solar power tower applications

Yunis KHAN[1,*], Deepak SINGH[2], Shailendra SINHA[3], K.S. BHOLE[2], D. APPARAO[4]

[1]*Department of Mechanical Engineering, Indian Institute of Technology, (ISM), Jharkhand, 826004, India*
[2]*Department of Mechanical Engineering, Sardar Patel College of Engineering, Andheri-west, Mumbai, Maharashtra, 400058 India*
[3]*Department of Mechanical Engineering, Institute of Engineering & Technology, Lucknow, Uttar Pradesh, 226021, India*
[4]*Department of Mechanical Engineering, Aditya Institute of Technology and Management, Andhra Pradesh, 532201, India*

ARTICLE INFO

Article history
Received: 29 July 2024
Accepted: 22 October 2024

Keywords:
Energy Analysis; Exergy Analysis; Exergoenvironmental Analysis; Helium Brayton Cycle; Parametric Analysis; Performance Comparison; Solar Power Tower; TCO_2 Cycle

ABSTRACT

This study introduces a combined cycle that captures solar energy from a solar power tower for power generation. The system couples a helium-based Brayton cycle (topping cycle) with a transcritical carbon dioxide cycle (bottoming cycle), where the latter recovers and uses the waste heat released from the Brayton process. A detailed investigation was carried out, incorporating energy, exergy, and exergoenvironmental evaluations, to assess the overall performance of the combined power plant. The findings demonstrated a significant improvement of 12.05% in the energy efficiency of the helium-based Brayton cycle when the transcritical carbon dioxide cycle was incorporated as a bottoming configuration. The plant's optimal operating parameters were identified, giving peak values of 23.2% for energy efficiency, 24.83% for exergy efficiency, and 14,930 kW for power output. A detailed examination of the solar subsystem components (receiver and heliostats) revealed the maximum exergy destruction occurs in these parts of the solar plant, totalling around 37,578 kW. The total exergy destruction across the plant was calculated to be 45,164 kW. The exergoenvironmental impact coefficient exhibited a substantial value of 4.028, primarily attributed to the lower exergy efficiency of the plant. Additionally, the energetic stability factor was found to be 0.2483. This research contributes to solar power tower integration, enhancing efficiency, and achieving a simplified system with fewer components compared to previous studies.

Cite this article as: Khan Y, Singh D, Sinha S, Bholeks KS, Apparao D. Exergy, energy, exergoenvironmental assessment of a novel combined helium Brayton cycle and transcritical CO_2 cycle for solar power tower applications. J Ther Eng 2026;12(1):1−20.

INTRODUCTION

The global energy demand grew by 2.2% in 2023, with emerging markets expected to drive further acceleration to 3.4% during the 2024-2026 period, despite the ongoing effects of the energy crisis and economic challenges, emphasizing the urgent need for secure and sustainable energy

***Corresponding author.**
*E-mail address: yuniskhan21@gmail.com

This paper was recommended for publication in revised form by Regional Editor Ahmet selim Dalklic

Published by Yıldız Technical University Press, İstanbul, Turkey
Yıldız Technical University. This is an open access article under the CC BY-NC license (http://creativecommons.org/licenses/by-nc/4.0/).

solutions [1,2]. Rising environmental challenges associated with greenhouse gas emissions, coupled with the progressive depletion of fossil fuel resources, have intensified the emphasis on sustainable energy alternatives, with particular attention directed toward the solar energy sector [3,4]. In response to the adverse environmental impacts of traditional energy sources, recent research has emphasized the development of clean and renewable technologies to reduce carbon footprints and mitigate climate change [5,6]. Solar energy, known as the most abundant renewable resource, is considered a reliable alternative to conventional energy, and its wide use is important to reduce global warming, cut fossil fuel dependence, and meet the rising demand for electricity [7]. According to recent studies, solar energy is widely used in everything from multi-generation systems that supply water, heating, cooling, and electricity to its integration with cutting-edge cycles that enhance energy efficiency and promote environmental sustainability [8–10].

To harness solar energy for electricity generation, two key technologies are used: Photovoltaic (PV) plants and concentrating solar power (CSP). CSP systems convert solar radiation into thermal energy, which is then used to drive thermodynamic cycles [11]. Using specialized mirror configurations or reflectors, CSP systems which are regarded as one of the most sustainable energy solutions achieve temperatures between 150 °C and 1500 °C. The power generation industry has shown a great deal of interest in these systems due to their increased cycle efficiency and capacity to produce high temperatures [12]. Recent studies indicate that among various CSP technologies, solar power tower (SPT) plants are advancing at a faster pace and gaining more attention than other CSP options [13]. In these plants, solar radiation is directed toward a central receiver by means of massive arrays of flat mirrors called heliostats. The heat transfer fluid (HTF) then gathers the thermal energy that has been absorbed. Because of their superior concentration ratios, solar power tower (SPT) systems can achieve temperatures up to 1500°C, which is significantly higher than parabolic trough collectors. Furthermore, the high source temperatures achieved enable these systems to function in hybrid configurations by coupling with the traditional fossil fuel plants, such as coal-fired Rankine cycles, thereby enhancing overall power generation efficiency.[14]. While solar power towers are capable of supporting thermodynamic cycles that operate within the elevated temperature range of 800 °C to 1200 °C, limited research has been conducted on their direct application for converting such high-temperature energy into electricity. The integration of solar power to with various thermodynamic cycles has garnered significant research attention over the past decade, focusing on operational features such as heliostat field configurations, different receiver types, power production systems, and HTF, with the aim of proposing and evaluating innovative power-generating units to achieve higher efficiency and develop a carbon-free energy system [15-18].

Depending on the heat source and operating temperature, solar power tower (SPT) plants can use either closed Brayton cycles or traditional Rankine cycles to convert thermal energy into electrical power. The supercritical carbon dioxide (sCO_2) Brayton cycle has garnered a lot of attention lately due to its advantageous characteristics, which include a critical temperature of nearly 31°C and a critical pressure of about 7,400 kPa. sCO_2 technology is very promising for effectively producing electricity from high-temperature heat sources because of its advantageous thermo-physical characteristics, compact design, and high efficiency. This allows for a low compression pressure ratio, which raises net output work [19]. Because of its chemical stability, non-flammability, affordability, non-toxicity, and environmental safety, the sCO_2 cycle is a great substitute. Instead of using a pump to keep the working fluid in a supercritical state, the supercritical Brayton cycle uses a compressor. Because of its high density, sCO_2 is especially appealing for waste heat recovery, enabling the design of compact turbo-machinery. Because of their increased effectiveness in high-temperature waste heat recovery applications, both transcritical and supercritical CO_2 cycles are becoming more and more popular [20]. Li et al. [21] provided a comprehensive classification of supercritical carbon dioxide (sCO_2) systems and emphasized their benefits in both nuclear and solar power applications. Gkountas et al. [22] used AlO_3 nanofluid to study heat transfer enhancement and discovered that adding printed circuit heat exchangers to sCO_2 systems reduced the pressure drop by 14% and exchanger length by 0.9%. Stainless steel works well up to 650 °C, while nickel-based alloys are better at higher temperatures, according to Chai and Tassuo's [23] evaluation of heat exchanger behavior in helium and sCO_2 Brayton cycles. After modeling five distinct sCO_2 cycle configurations for solar power tower (SPT) systems, Al-Sulaiman and Atif [24] found that the recompression cycle was the most effective, achieving 52% efficiency. To further improve the SPT system's performance, the same researchers optimized the heliostat field layout in subsequent work [25].

In hybrid heat source systems, stand et al. [26] examined the integration of an sCO_2 cycle with an organic Rankine cycle (ORC) in a hybrid solar power tower (SPT) plant, achieving a second law efficiency of 26.6%. With a product cost rate of $0.71/s, Hashemian and Noorpoor's [27] biomass–solar powered multi-generation system improved energy efficiency from 14% to 16.53% after optimization. With a 14.46% exergy efficiency, Zainul et al. [28] created a hybrid system for coastal applications that combines solar, wind, and ocean thermal energy. The application of NSGA-II optimization improved overall performance while reducing environmental impacts. Yang et al. [29] examined a biomass-solar system, emphasizing enhancements in solar collector and absorption chiller efficiency while minimizing environmental impact through ICE and gasifier optimization. Through the use of NSGA-II, Rahimimotlagh and Ahmadi [30] combined solar dish collectors with

compressed air storage and absorption chillers, resulting in a round-trip efficiency of 62.69% and an annual reduction of 3,810 tons of CO_2 emissions. Using a two-stage ORC, Qi et al. [31] stabilized biomass-solar energy while identifying important evaporator and condenser upgrades to increase energy efficiency and lessen environmental impact. Zhou et al. [32] combined organic Rankine, ejector refrigeration, and organic flash cycles into a solar desalination system, producing 5.89 kg/h of freshwater, 143.4 kW of net power, and approximately 66.85 kW of cooling capacity. The total energy destruction was reported to be 892.8 kW. By maximizing condenser costs and environmental performance, Cavalcanti [33] assessed a cogenerative system and demonstrated a 4.2% increase in electricity production. Su et al. [34] optimized a multistage Brayton cycle for solar power, boosting exergy efficiency to 25.92% and lowering electricity costs while promoting sustainability goals. Helium was determined to be the best option by Javanshir et al. [26], who evaluated the thermodynamic performance of basic and regenerative Brayton cycles for SPT plants using a variety of working fluids. By creating a triple-coupled cycle that combines an air Brayton cycle, an ORC, and SRC for SPT applications, Sachdeva and Singh [15] were able to reach a maximum efficiency of 33.15%. In their comparison of CO2-based binary mixtures, Guo et al. [35] discovered that the CO2/Xenon intercooling cycle performed better than sCO2 with an exergy efficiency that was 1.32% higher. Trevisan et al. [36] addressed the temperature limitations of a recompression sCO_2 cycle by using air as the heat transfer fluid, which led to a levelized cost of electricity (LCOE) of 100 $/MWh. Niu et al. [37] found the CO2-propane mixture performs best at high ambient temperatures in an SBC-based SPT. Wan et al. [38] implemented an off-design control strategy in a recompression supercritical CO_2 (R-sCO_2) cycle, achieving a power increase of 1.02%. Lu et al. [39] emonstrated that the recompression cycle model, configured with an optimized bypass fraction, exhibits superior performance compared to the regenerative cycle under the off-design operating conditions. Bai et al. [40] optimized the SF6-CO2 mixture for solar-powered SBCs, while Ma et al. [41] identified the CO2-Xe mixture as the top thermodynamic performer in the sCO2 cycle. Kademi et al. [42] discovered an exergy efficiency of 61.8% for a multigenerational system employing ORC and sCO2 Brayton cycles, while Liu et al. [43] computed a maximum daily efficiency of 26.26% for a sCO2-based SPT plant. Butane was found to be the most appropriate working fluid in another study that optimized an ORC in conjunction with a vapor compression refrigeration (VCR) system, attaining 33.7% efficiency with a 4.9-year payback period [44]. R1224yd(Z) was found to be the most efficient working fluid. Khan et al. [45] reported that the thermal efficiency of a combined organic Rankine cycle and partial cooling supercritical CO_2 cycle increases from 35.16% to 55.43% with increasing solar irradiation, along with a power output enhancement from 188 kW to 298.5 kW.

For SPT applications, the majority of the referenced literature has mostly concentrated on either the more modern sCO2 cycle or the more conventional steam Rankine cycle. There is a glaring research gap because the recuperated helium Brayton cycle (HBC), which is well-known for its simplicity and high efficiency at operating temperatures above 500 °C, has gotten relatively little attention. With over 20 studies on CSP systems published in the last three to four years, the literature review shows a notable increase in research on sCO_2 Brayton cycles for SPTs. Helium consistently outperforms carbon dioxide (CO_2) and other fluids in SBC systems for SPT applications, according to a number of studies [5, 18, 26] that have also examined various gases as working media in supercritical Brayton cycles.

The literature review clearly indicates that although HBCs are technologically advanced, their application is limited due to the high operating temperatures required for efficiency. Hybrid Brayton cycles (HBCs) achieve optimal performance predominantly at high temperatures, owing to their substantial back work ratio. In a simple recuperative Brayton configuration, helium provides notable economic benefits compared to other working fluids [46]. At high temperatures, helium's elevated heat capacity lowers the amount of required mass flow rate, which in turn reduces component size and cost, improving its economic viability. Since solar power tower (SPT) plants typically operate under such conditions, helium has been found to perform better than carbon dioxide and other fluid operating at this temperature [47].

The literature offers limited evidence regarding the application of hybrid Brayton cycles (HBC) in solar thermal power plants. Because organic working fluids have favorable thermodynamic qualities and operating characteristics at low temperatures, Organic Rankine cycles (ORCs) are generally preferred for low-temperature applications. However, because it provides better temperature-matching glide in the evaporator, the TCO_2 cycle is a better option than ORC for recovering heat from high-temperature sources. Organic fluids, however, may cause pinch-point temperature challenges within the evaporator. From a thermodynamic standpoint, the transcritical CO_2 (TCO_2) cycle has demonstrated superior heat rejection performance relative to the organic Rankine cycle (ORC) [48].

Thus, this study uses thermodynamic and exergoenvironmental analysis to evaluate a novel system that combines the HBC with a TCO_2 cycle. By utilizing helium as the high temperature operating fluid, the performance of the supercritical Brayton cycle (SBC) has seen significant enhancements in its performance. For simple Brayton cycle (SBC) systems, a considerable portion of thermal energy is rejected to the surroundings during the cooling of the working fluid before compression, most notably within the 150–250 °C range. The TCO_2 cycle is purposefully used as a bottoming cycle to reduce this waste, efficiently recovering the waste heat from the HBC. Given the TCO_2 cycle's exceptional adaptability in waste heat recovery, as highlighted by

earlier studies [49-51], this integrated approach is not only effective but also a promising development in solar thermal applications.

Based on the explanation above, the current study's objectives are as follows:

1. To propose and develop a novel integrated power generation system that combines the helium Brayton cycle as the topping cycle with the transcritical CO_2 cycle as the bottoming cycle, thereby enhancing solar energy utilization in a solar power tower plant.
2. To thoroughly evaluate the proposed system's energy, exergy, and exergoenvironmental aspects, with an emphasis on reducing negative effects on the environment while maximizing system performance.
3. To carry out a thorough parametric analysis in order to identify the key variables influencing the system's performance and the ideal operating conditions.
4. To emphasize the novel contribution of this study by replacing the conventional exergoeconomic analysis with a more relevant exergoenvironmental analysis [3,28, 32,52,53], thus addressing both efficiency and environmental impact.

SYSTEM DESCRIPTION

Figure 1 presents the current study, and Figure 2 displays the temperature–entropy (T–s) curve of the proposed thermodynamic system. In the SPT configuration, air is used as the heat transfer fluid (HTF) to absorb solar radiation, and the internal heat exchanger (IHE) transfers this heat to the HBC, which operates as the topping cycle. Notably, helium has been chosen as the working fluid in the topping cycle, replacing the conventional supercritical CO_2 [24, 25]. Previous research indicates that helium Brayton cycles can reach higher efficiencies than CO_2 Brayton cycles when the compressor pressure ratio is less than 2.5 and the turbine inlet temperature exceeds 550 °C. Helium also outperforms CO_2 at elevated turbine inlet temperatures, which are found in solar plants utilizing central receivers [25, 26]. Additionally, helium has several distinctive qualities that make it appropriate for power cycles. Among its most noteworthy characteristics are its chemical inertness and low specific gravity [25]. The bottoming transcritical CO_2 (TCO_2) cycle operates by utilizing the leftover waste heat from the helium Brayton topping cycle through a waste heat recovery unit (WHRU). The ORC and TCO_2 cycles are two effective ways to turn low-grade heat into electricity. Because of its simplified configuration and ability to function effectively at low pressure, the ORC lowers system costs. Its versatility is further increased by its ability to adapt to different heat sources, provided that the right working fluids are found. One significant drawback, though, is the existence of the pinch point temperature difference shown in Figure 3(a), which represents the lowest temperature differential between the hot and cold fluids. Because of the significant mismatch between the two working fluids, this phenomenon introduces irreversibility into the heat exchanger. Transcritical CO2 turns out to be an excellent substitute for this restriction. The pinch point temperature difference, or the lowest temperature differential between the hot and cold fluids, is removed during the transcritical heating process. This is demonstrated in Figure 3(b), where the working fluid's temperature contour slides to provide a more advantageous alignment of the hot and cold fluid curves. This feature improves overall system performance by reducing irreversibility and getting around the pinch point temperature difference limitation.

The current combined system operates systematically as follows: Helium first cools in the precooler, putting it in state 1. After that, it passes through the compressor, which raises its temperature and pressure to state 2. In state 3, heat is absorbed in the recuperator by the cold, high-pressure helium stream. State 4 is reached when the temperature is further raised by the residual heat from the intermediate heat exchanger (IHE). The stream of high-temperature, high-pressure helium now enters the turbine, expands, and changes into state 5. After passing through the recuperator and exchanging heat with the compressor's cold stream, the medium-temperature helium stream eventually reaches state 6. At state 6, the helium has enough energy to drive a bottoming cycle, which is aided by the WHRU and involves heat exchange with the bottoming cycle's working fluid, carbon dioxide. After reaching state 7, the helium stream passes through a cooler to expel any last bits of heat before going back to state 1. At the same time, heat from the helium inside the WHRU is absorbed by the high-pressure CO2 stream, which was initially in state 11, changing to state 8. The CO2 reaches state 9, where its temperature and pressure decrease, as a result of ongoing expansion in the transcritical turbine. Following expansion, the CO2 undergoes a phase transition as it passes through the condenser, losing any heat that remains and arriving at state 10. The cycle is restarted by pumping the CO2, which is now in a low-temperature, low-pressure state, back to state 11. The system's optimal energy use and effective heat transfer are guaranteed by this cyclic process.

PERFORMANCE ASSESSMENT

Exergy and Energy Analysis

The analysis of the present system was carried out based on the following assumptions: (1) all components operate under steady-state conditions; (2) pressure losses in the components are taken as given in Table 1; (3) kinetic and potential energy contributions are neglected; and (4) the isentropic efficiencies of the turbine, pump, and compressor are adopted from the values reported in Table 1. The overall system considered for thermodynamic evaluation includes the helium Brayton cycle and the transcritical CO_2 (HBC–TCO_2) power cycle together with the solar sub-system. In the simulation performed using EES, each component is modeled as a separate

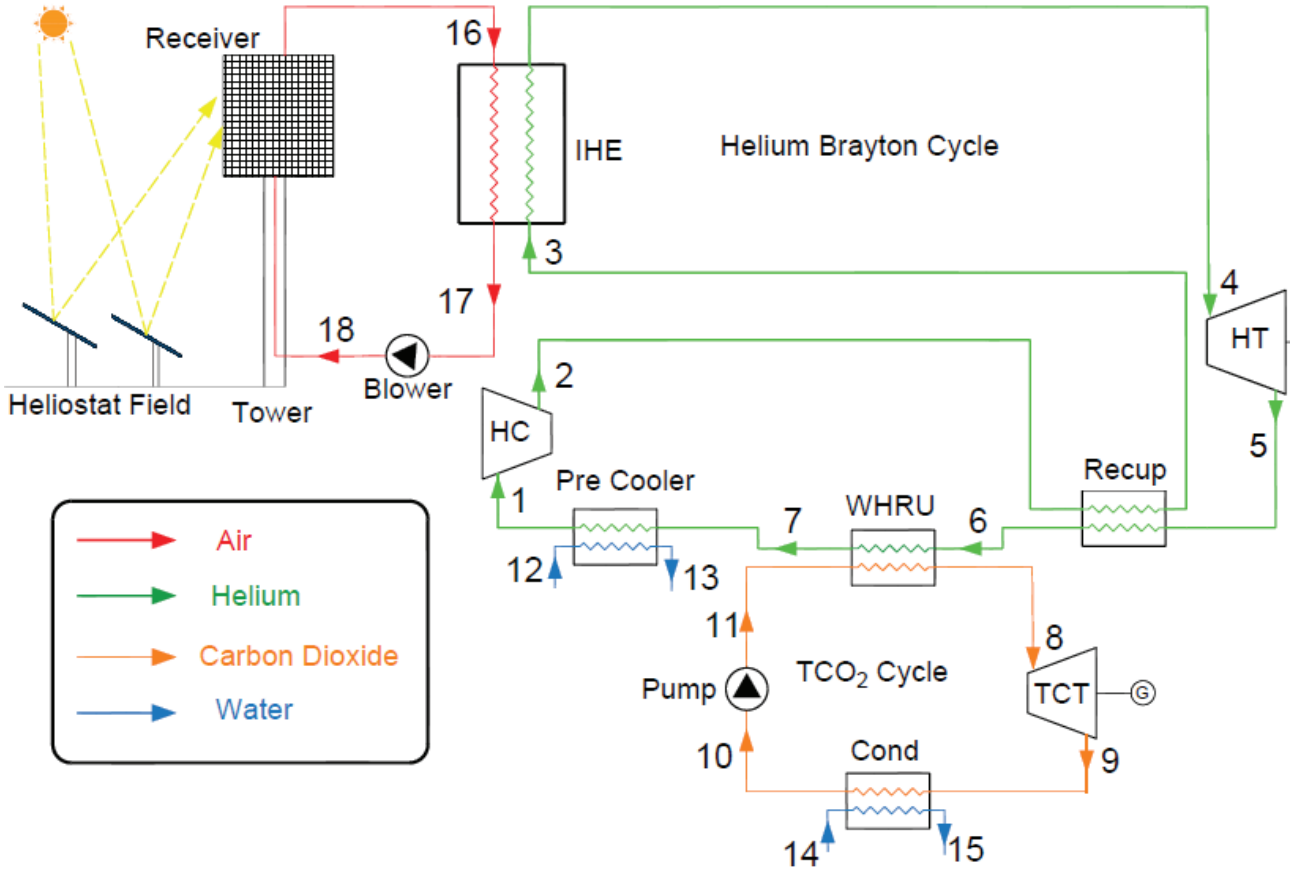

Figure 1. Proposed system diagram.

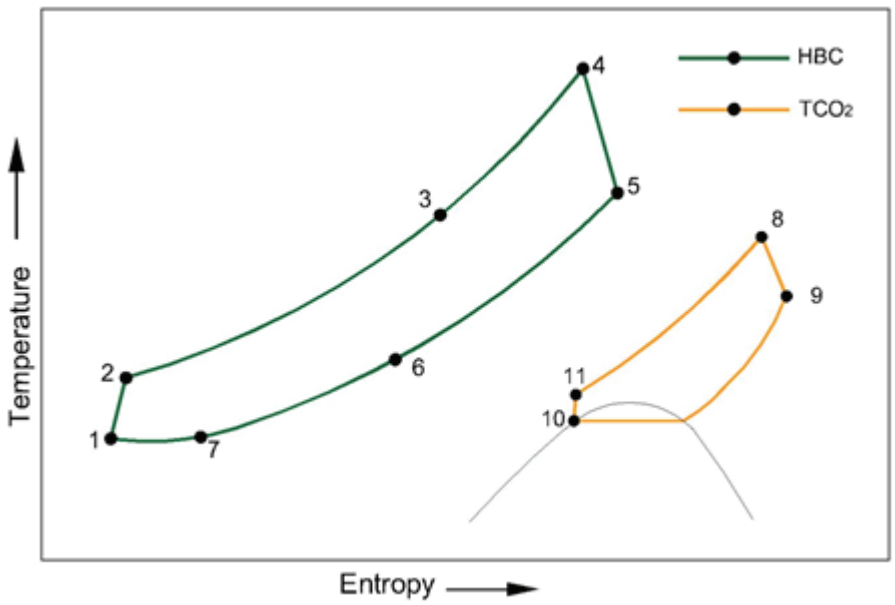

Figure 2. Temperature-entropy (T-s) diagram.

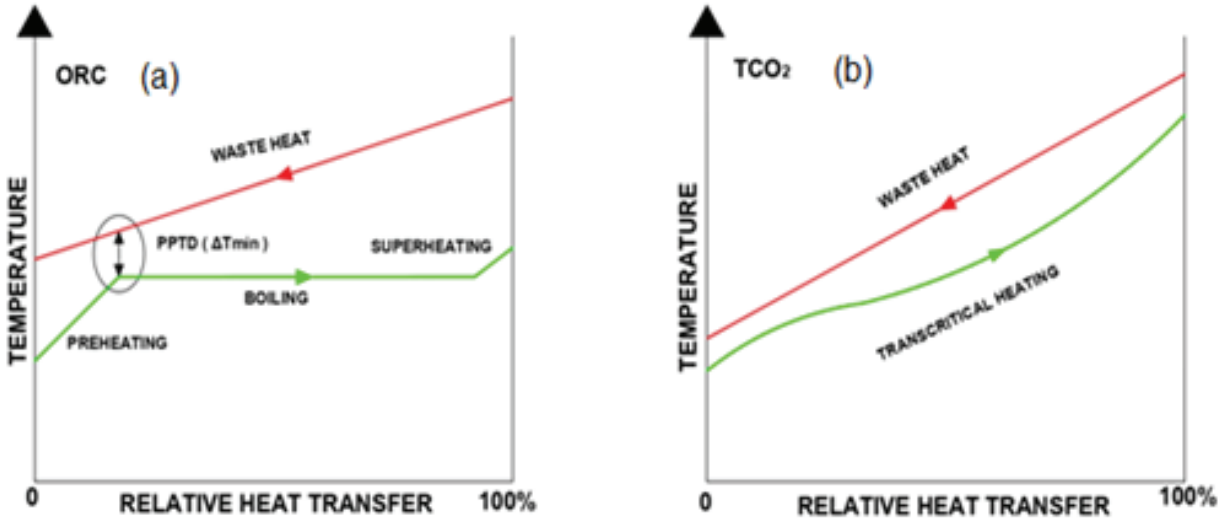

Figure 3. Temperature and heat transfer characteristics of (a) ORC, (b) TCO_2 cycle.

thermodynamic system. The governing energy and exergy balances for a control volume under steady-state conditions are expressed through the following equations:

$$\dot{Q}_{CV} - \dot{W}_{CV} + \sum(\dot{m}_i h_i) - \sum(\dot{m}_e h_e) = 0 \quad (1)$$

$$\dot{ED} = \dot{EX}_{in} - \dot{EX}_{out} \quad (2)$$

Where, $\dot{E}D$ is exergy destruction rate within the thermodynamic component. The control volume's heat and work interactions are represented by $\dot{W}_{CV}$ and $\dot{Q}_{CV}$, respectively.

The physical exergy of a fluid stream is calculated by measuring the exergy rate associated with its flow. This calculation excludes the contributions from kinetic energy, potential energy, and chemical exergy, as the suggested system lacks chemical concentration.

$$\dot{EX}_j = \dot{m}\cdot[(h_j - h_0) - T_0(s_j - s_0)] \quad (3)$$

Here, j indicates a specific state, and $\dot{E}X_j$ denotes the physical exergy at that state. The heliostat field and the receiver make up the solar subsystem. The receiver uses multiple heliostats, each with an aperture area designated as A_{hel}, to concentrate and direct solar radiation onto the primary receiver. The heliostat field efficiency defines the fraction of solar thermal energy from direct normal irradiation (DNI) that is delivered to the central receiver. The efficiency of the field depends on its configuration, while the variability in the solar energy received is linked to time of day and geographical location. The usable heat received by the receiver represents only a fraction of the total solar irradiation as remaining solar energy is lost. The calculation for this is given by [27];

$$\dot{Q}_{rec,in} = \eta_{field}\cdot\dot{Q}_{Sun} = \eta_{field}\cdot DNI \cdot A_{hel} \cdot N_{hel} \quad (4)$$

Where, η_{field} is the heliostat field efficiency [28];

$$\eta_{field} = \eta_{cos}\cdot\eta_{s\&b}\cdot\eta_{int}\cdot\eta_{att}\cdot\eta_{ref} \quad (5)$$

Where, η_{cos}, η_{int}, $\eta_{s\&b}$, η_{att}, η_{ref} represents, in that order, the efficiency of the cosine effect, interception efficiency, shading and blocking efficiency, atmospheric attenuation efficiency, and heliostat reflectivity efficiency. It should be noted that this research uses actual data from an operating solar power plant instead of calculating these characteristics theoretically.

Heat losses from the receiver occur through reflection, conduction, and convection given by ($\dot{Q}_{rec,loss}$), while the absorbed heat is represented as ($\dot{Q}_{rec,in}$). The net heat transferred to the heat transfer fluid (HTF), which is air, is given as $\dot{Q}_{rec,net}$. The receiver efficiency is then calculated as [29]:

$$\eta_{rec} = \frac{\dot{Q}_{rec,net}}{\dot{Q}_{rec,in}} \quad (6)$$

$$\dot{Q}_{rec,in} = \dot{Q}_{rec,net} + \dot{Q}_{rec,loss} = \dot{m}_{air}(h_{16} - h_{17}) + \dot{Q}_{rec,loss} \quad (7)$$

The exegetic and energetic balance equations for each component are given in Table 2. Together with the input data mentioned in Table 1, these relationships are a crucial part of the simulation code that was written using EES software. The program uses its built-in property function libraries to retrieve thermodynamic properties in order to evaluate the unknown parameters. These include exergy rates for individual streams, heat and work interactions, and state-point thermodynamic properties. The energy and exergy efficiencies of the solar power plant are defined as the ratio of the net output power to the respective energy or exergy input from solar irradiation incident on the heliostat field [29]:

$$\eta_{th,overall} = \frac{\dot{W}_{net}}{\dot{Q}_{Sun}} \quad (8)$$

$$\eta_{ex,overall} = \frac{\dot{W}_{net}}{\dot{Q}_{Sun}\cdot\left(1-\frac{T_0}{T_{ref,Sun}}\right)} \quad (9)$$

Where $T_{ref\ .Sun}$ denotes the apparent temperature of the sun [29]. $\dot{W}_{net}$ is the plant's net power output calculated as:

$$\dot{W}_{net} = \dot{W}_{HT} - \dot{W}_{HC} + \dot{W}_{TCO_2\ turbine} - \dot{W}_{pump} \quad (10)$$

For the power production unit, the combined cycle (HBC-TCO_2 cycle) efficiency can be described as [21]:

$$\eta_{th,comb} = \frac{\dot{W}_{net}}{\dot{Q}_{IHE}} \quad (11)$$

$$\eta_{ex,comb} = \frac{\dot{W}_{net}}{(\dot{EX}_{16}-\dot{EX}_{17})} \quad (12)$$

Where, $(\dot{EX}_{16} - \dot{EX}_{17})$ denotes the amount of total exergy input available for the combined cycle [21].

Exergoenvironmental Analysis

Alongside thermal analysis, assessing the environmental impact of power systems is essential for achieving long-term sustainability. Conventional energy and exergy-based thermodynamic analyses alone prove insufficient for this purpose. Hence, integrated multigenerational systems turn to exergy for comprehensive environmental assessments and sustainability evaluations. An analysis of the effects of exergy efficiency and destruction rates on the environment forms the direction of exergoenvironmental analysis. For this assessment, specific exergoenvironmental performance parameters, detailed in reference [5], are employed. Beyond conventional thermodynamic analyses, this holistic approach enables a more nuanced understanding of the sustainability and environmental implications of power systems.

An important metric that sheds light on the environmental effects of a thermal system and provides a framework for formulating plans to mitigate these effects by reducing irreversibility is the exergoenvironmental impact factor (f_{ei}). The ratio of the total energy supplied at the system inlet to the total energy destroyed in the system is how this parameter is expressed. In essence, it quantifies the extent to which a thermal system affects the environment and, on the other hand, shows how this impact might be lessened by increasing overall efficiency. Idealistically, when the exergoenvironmental impact factor (f_{ei}) value is 0, the system indicates no irreversibility.

Mathematically, it is represented as:

$$f_{ei} = \frac{\dot{ED}_{total}}{\dot{EX}_{Sun}} \quad (13)$$

The exergoenvironmental impact coefficient (C_{ei}), defined as the reciprocal of exergy efficiency, is an important measure for the present system. Better performance is indicated by a lower value of this coefficient, whereas an ideal condition with no exergy destruction is represented by a value of one.

Mathematically, it can be expressed as:

$$C_{ei} = \frac{1}{\eta_{ex,overall}} \quad (14)$$

One metric for determining whether a system has a positive or negative impact on the environment is the exergoenvironmental impact index (θ_{ei}). A lower value of this index suggests that the system exhibits superior environmental performance. In essence, a lower exergoenvironmental impact index number means that the system is performing better in terms of limiting its influence on the environment.

Mathematically, it is represented as:

$$\theta_{ei} = C_{ei}\cdot f_{ei} \quad (15)$$

For best results, the exergy stability factor (f_{es}) should ideally be "one" or approaching "one.". This indicates that, from an exergoenvironmental perspective, the system is performing exceptionally well. In other words, when the exergy stability factor is close to or equal to 'one,' it signifies that the system is achieving a high level of stability and efficiency concerning exergy considerations in the environmental context.

It can be represented as;

$$f_{es} = \frac{\dot{EX}_{out}}{\dot{EX}_{out}+\dot{ED}_{total}} \quad (16)$$

The exergoenvironmental impact improvement parameter θ_{eii} serves as a crucial metric in evaluating a system's harmony with environmental conditions. In contrast to the exergoenvironmental impact index, a higher value of the θ_{eii} parameter indicates better environmental performance. An increase in θ_{eii} reflects a stronger positive influence of the system on environmental conditions.

Mathematically, it is expressed as:

$$\theta_{eii} = \frac{1}{\theta_{ei}} \quad (17)$$

The exergetic sustainability index θ_{est} is obtained by multiplying the exergoenvironmental impact improvement parameter with the exergetic stability factor. A higher θ_{est} value reflects a system with stronger environmental benefits, whereas a lower value indicates adverse environmental effects within the studied system. In essence, the exergetic sustainability index provides a crucial measure of a system's environmental performance, with an elevated value indicating a more sustainable and eco-friendly operation.

Mathematically, it can be expressed as:

$$\theta_{est} = \theta_{eii}\cdot f_{es} \quad (18)$$

The exergoenvironmental analysis was performed through the utilization of modeling equations, and the results were computed employing computational techniques with Engineering Equation Solver (EES).

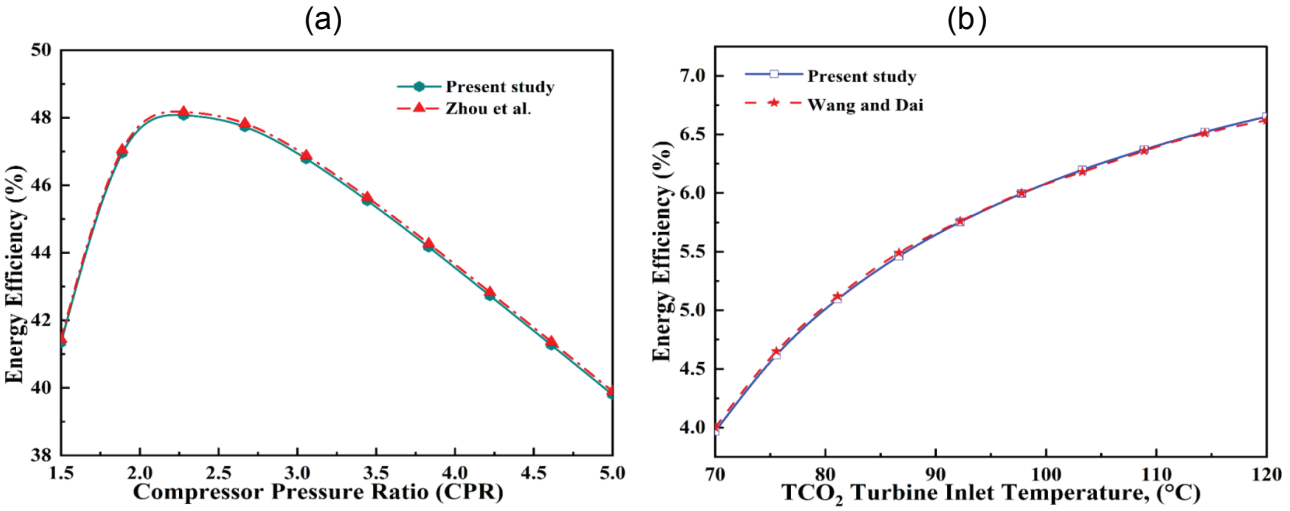

Figure 4. Validation for (a) helium Brayton cycle, (b) TCO_2 cycle.

Validation

To validate the modeling approach, the results of the two developed models, the tCO_2 cycle and the HBC cycle are compared with data available in reputable literature. Figure 4(a) presents the efficiency values of the standalone HBC system from this study alongside those reported by Zhou et al. [21]. Notably, the data discrepancy is within a reasonable range—just 0.24%. For the bottoming TCO_2

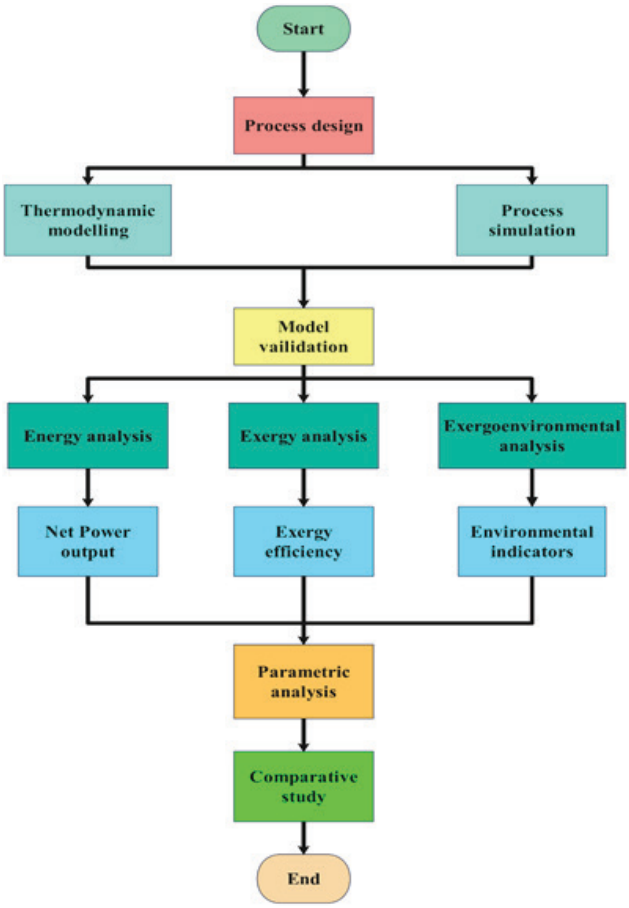

Figure 5. The flow diagram for the current study's solution and structure.

Table 1. Simulation data for the present study [3,9,17]

Parameters	Value
Atmospheric temperature (T_o)	25 °C
Atmospheric pressure (P_o)	101.3 kPa
Apparent Sun temperature (T_{Sun})	4500 K
Heat exchanger effectiveness (ε)	0.9
Air inlet temperature at IHE (T_{16})	1125 °C
Direct normal irradiation (DNI)	850 W/m^2
Count of heliostats (N_{hel})	624
Receiver aperture area (A_{rec})	68.1 m^2
Efficiency of heliostat field (η_{field})	0.6428
Every heliostat's reflecting area (A_{hel})	9.45 × 12.84 m^2
Efficiency of the receiver (η_{rec})	0.75
Isentropic efficiency of helium compressor (η_{HC})	0.89
Isentropic efficiency of helium turbine (η_{HT})	0.93
TCO_2 turbine's isentropic efficiency ($\eta_{TCO_2\ turbine}$)	0.8
Pump's isentropic efficiency (η_{Pump})	0.7
Helium Turbine's inlet temperature (T_4)	800 °C
TCO_2 turbine's inlet temperature (T_8)	180 °C
Pressure at the helium compressor's inlet (P_1)	2500 kPa
Compressor pressure ratio (CPR)	2.3
Pump pressure ratio (PPR)	3.033
Intermediate heat exchanger's pressure loss	2%
Pinch point temperature difference in WHRU	10 °C
Loss of pressure in the recuperator/WHRU	1%
Pinch point temperature difference in condenser	5 °C

Table 2. Energy-exergy analysis equations for every component

Components	Energy balance equation	Exergy balance equation
Receiver	$\dot{Q}_{rec,in} = \dot{m}_{air}(h_{16} - h_{17}) + \dot{Q}_{rec,loss}$	$\dot{E}X_{17} + \dot{Q}_{rec,in}\cdot\left(1-\frac{T_0}{T_{ref,hel}}\right) = \dot{E}X_{16} + \dot{Q}_{rec,loss}\cdot\left(1-\frac{T_0}{T_{rec}}\right) + \dot{E}D_{rec}$
Heliostat field	$\dot{Q}_{rec,in} = \eta_{field}\cdot DNI \cdot A_{hel} \cdot N_{hel}$	$\dot{Q}_{Sun}\cdot\left(1-\frac{T_0}{T_{ref,Sun}}\right) = \dot{Q}_{rec,in}\cdot\left(1-\frac{T_0}{T_{ref,hel}}\right) + \dot{E}D_{hel}$
Helium compressor	$\dot{W}_{HC} = \dot{m}_{He}\cdot(h_2 - h_1)$ $\eta_{HC} = \frac{(h_{2s} - h_1)}{(h_2 - h_1)}$	$\dot{E}X_1 = \dot{E}X_2 - \dot{W}_{HC} + \dot{E}D_{HC}$
Helium turbine	$\dot{W}_{HT} = \dot{m}_{He}\cdot(h_4 - h_5)$ $\eta_{HT} = \frac{(h_4 - h_5)}{(h_4 - h_{5s})}$	$\dot{E}X_4 = \dot{E}X_5 + \dot{W}_{HT} + \dot{E}D_{HT}$
IHE	$\dot{Q}_{IHE} = \dot{m}_{air}\cdot(h_{16} - h_{17}) + \dot{m}_{He}\cdot(h_4 - h_3)$	$\dot{E}X_{16} - \dot{E}X_{17} = \dot{E}X_4 - \dot{E}X_3 + \dot{E}D_{IHE}$
Recuperator	$(h_3 - h_2) = (h_5 - h_6)$ $\varepsilon_{Recuperator} = \frac{(T_3 - T_2)}{(T_5 - T_2)}$	$\dot{E}X_5 - \dot{E}X_6 = \dot{E}X_3 - \dot{E}X_2 + \dot{E}D_{Recuperator}$
WHRU	$\dot{m}_{He}\cdot(h_6 - h_7) = \dot{m}_{CO2}\cdot(h_8 - h_{11})$	$\dot{E}X_6 - \dot{E}X_7 = \dot{E}X_8 - \dot{E}X_{11} + \dot{E}D_{WHRU}$
TCO_2 turbine	$\dot{W}_{TCO_2\ turbine} = \dot{m}_{CO2}(h_8 - h_9)$ $\eta_{TCO_2\ turbine} = \frac{(h_8 - h_9)}{(h_8 - h_{9S})}$	$\dot{E}X_8 = \dot{E}X_9 + \dot{W}_{TCO_2\ turbine} + \dot{E}D_{TCO_2\ turbine}$
Pump	$\dot{W}_{Pump} = \dot{m}_{CO2}(h_{11} - h_{10})$ $\eta_{Pump} = \frac{(h_{11s} - h_{10})}{(h_{11} - h_{10})}$	$\dot{E}X_{10} = \dot{E}X_{11} - \dot{W}_{Pump} + \dot{E}D_{Pump}$
Precooler	$\dot{m}_{air}\cdot(h_7 - h_1) = \dot{m}_{water}\cdot(h_{13} - h_{12})$	$\dot{E}X_7 - \dot{E}X_1 = \dot{E}X_{13} - \dot{E}X_{12} + \dot{E}D_{Preooler}$
COND	$\dot{m}_{CO2}\cdot(h_9 - h_{10}) = \dot{m}_{water}\cdot(h_{15} - h_{14})$	$\dot{E}X_9 - \dot{E}X_{10} = \dot{E}X_{15} - \dot{E}X_{14} + \dot{E}D_{COND}$

cycle, we conducted a validation using the results presented in Figure 4(b), as reported by Wang and Dai [30], who employed the same input conditions. The comparison indicates a slight variation of less than 1% in the results, which is also regarded as acceptable. In summary, these validations serve to affirm the accuracy and reliability of our modeling technique. The flow diagram for the solution and structure of the current study is displayed in Figure 5.

RESULTS AND DISCUSSION

The system simulation was performed using the assumptions and input parameters listed in Table 1. To provide a detailed understanding of the cycle's energy and exergy behavior, the results obtained at optimal operating conditions for all subsystems are summarized in Table 3. Based on a solar irradiation input of 64,358 kW, the energy analysis shows that the plant's total power output is 14,930 kW, which translates to an overall energy efficiency of 23.20%. At 22,989 kW, or 35.72% of the solar input, the heliostat field is responsible for the greatest amount of energy loss. This outcome underlines the importance of an efficient heliostat field design in solar power tower plants. The combined HBC–TCO_2 cycle records an energy efficiency of 48.11%. High-grade energy with a source temperature of roughly 4500 K is produced by solar radiation [29]. Significant irreversibilities happen when this energy reaches the receiver at almost 1125 °C, and exergy analysis shows that the heliostat field has the highest exergy destruction. The heliostat field efficiency under these circumstances is determined to be 64.24%. Because the system does not involve combustion, which is a major source of irreversibility in conventional plants, the temperature difference between helium and the heat transfer fluid (air) in the intermediate heat exchanger (IHE) remains low. This condition allows the combined cycle to reach an exergy efficiency of 66.31%. Despite this improvement, the plant's overall energy efficiency is still constrained because of the substantial damage to the heliostat field and receiver. According to a component-level analysis, the heliostat field has the highest energy destruction at 21,465 kW, while the precooler has the lowest at 405.9 kW, accounting for 47.52% of the total. At 97.25%, the helium turbine exhibits the highest energy efficiency of any component. Together, the energy and exergy analysis

Table 3. Results of exergy-energy evaluation under the specified operating parameters*

Subsystems	Energetic Assessment				Exergetic Assessment			
	Input (kW)	Output (kW)	Loss (kW)	Energy efficiency	Input (kW)	Output (kW)	Loss (kW)	Exergy efficiency
Heliostat field	64358	41369	22989	64.27%	60094	38628	21465	64.27%
Solar receiver	41369	31027	10342	75%	38628	22515	16113	58.28%
HBC	31027	13365	17662	43.07%	22515	13365	9150	59.36%
TCO_2 cycle	13261	1565	11696	11.8%	3698	1565	2133	42.32%
Combined cycle	31027	14930	16097	48.11%	22515	14930	7586	66.31%
Overall power plant	64358	14930	49428	23.2%	60094	14930	45164	24.83%

*T_4 = 800 °C, CPR = 2.3, PPR = 3.033, T_8 = 180 °C, DNI = 850W/m²

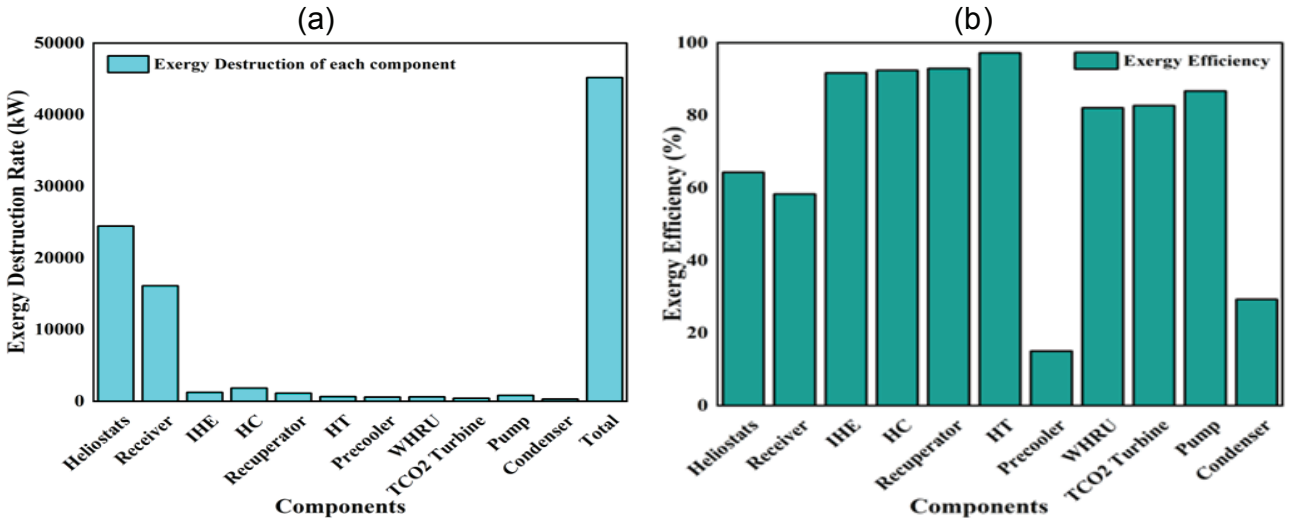

Figure 6. Each components (a) exergy destruction, (b) exergy efficiency.

results provide a thorough evaluation of the system's operation and the allocation of losses and efficiencies. The exergy destruction rates and efficiencies of individual components are further presented in Figures 6(a) and 6(b), which provide a clear representation of their contributions to overall system behavior.

In addition, Table 4 lists the values of the exergoenvironmental performance metrics in the basic case. Observing the plant's below-average exergy efficiency, it becomes evident that the exergoenvironmental effect coefficient is notably higher, measuring at 4.028. This result highlights that there is still a great deal of room to reduce the negative environmental effects of the system. An ideal degree of environmental stability is indicated by an exergetic stability factor of 1. The actual value, however, is 0.2483, indicating that this system continues to have an impact on environmental stability. In conclusion, the results emphasize the need for enhancements meant to lessen the system's negative effects on the environment and increase its sustainability. Table 5 lists the thermodynamic properties at each state with respect to Figure 1. These data present a detailed overview of the system's thermodynamic condition at the key state points. This precise data serves as the cornerstone for precise modeling and analysis, offering insights into the efficiency and dynamic behavior of the power plant.

Table 4. Values of the exergoenvironmental performance parameters at base case

Parameters	Values
Exergoenvironmental impact index (θ_{ei})	3.028
Exergoenvironmental impact coefficient (C_{ei})	4.028
Exergetic sustainability index (θ_{est})	0.0819
Exergoenvironmental impact factor (f_{ei})	0.7517
Exergy stability factor (f_{es})	0.2483
Exergoenvironmental impact improvement (θ_{eii})	0.3302

Table 5. The proposed system's mass flow rates and thermodynamic parameters

State	Working Fluid	ṁ(kg/s)	P (kPa)	T (°C)	h (kJ/kg·°C)	s (kJ/kg·°C)	ĖX (kW)
1	He	20.11	2500	30	34.04	-6.569	39014
2	He	20.11	5833	167.4	757.7	-6.386	52110
3	He	20.11	5774	494.6	2455	-3.483	68404
4	He	20.11	5659	800	4040	-1.703	89040
5	He	20.11	2577	530.7	2634	-1.569	60727
6	He	20.11	2551	203.7	936.1	-4.259	43190
7	He	20.11	2525	73.28	258.8	-5.898	39492
8	CO_2	56.47	21879	180	56.01	-0.7824	16353
9	CO_2	56.47	7214	87.83	3.138	-0.7453	12743
10	CO_2	56.47	7214	30	-204	-1.401	12092
11	CO_2	56.47	21879	63.28	-178.8	-1.39	13323
12	Water	105.2	101.3	25	104.8	0.3669	0
13	Water	105.2	101.3	35	146.7	0.5049	72.19
14	Water	279.6	101.3	35	146.7	0.5049	191.9
15	Water	279.6	101.3	25	104.8	0.3669	0
16	Air	46.2	101.3	544.6	841.8	6.741	10690
17	Air	46.2	101.3	1125	1513	7.359	33205

Additionally, the impact of various variables on the power plant performance has been assessed conducted through a parametric analysis. This analysis involves varying one parameter at a time while keeping the other parameters, as listed in Table 1, constant. The following sections in this report segment delve into a thorough exploration of the individual effects of each parameter.

Effect on Performance of The System Compressor Pressure Ratio

Since it has a direct impact on the selection of compressor material and related expenses, the compressor pressure ratio (CPR) is a crucial variable being studied. As depicted in Figure 7(a), a discernible trend in energy efficiency emerges, initially ascending and then consistently descending. Reaching 48.32% for the combined cycle and 43.12% for the standalone configuration, the maximum energy efficiency is achieved at a CPR of 2.3. A substantial 12.05% enhancement in energy efficiency with the integration of the TCO_2 cycle into the basic HBC (standalone). In evaluating the performance of the combined cycle CPR emerges as a key factor. Energy and exergy efficiencies show an initial ascent, peaking at a CPR of 2.3 with energy efficiency at 47.87% and exergy efficiency at 65.56%. However, beyond CPR 2.3, both efficiencies decline. The interplay between expansion and compression work explains this behavior. Both increase together when the CPR is less than 2.3, but after that, the increase in compression work is greater than the increase in expansion work, which lowers the combined cycle's efficiency and net output. The analysis emphasizes how important CPR is in determining the power plant configuration's overall efficiency landscape.

Figure 7(b) shows the influence of CPR on the energy and exergy efficiencies of the HBC–TCO_2 combined cycle. Both efficiencies rise with increasing CPR, reach their maximum at 2.3, and then gradually decrease, consistent with the earlier discussion. The maximum values recorded are 47.87% for energy efficiency and 65.56% for exergy efficiency. Figure 7(c), illustrating variations in energy, exergy, and network output for the power plant (SPT-HBC-TCO_2 cycle), a similar pattern emerges as in Figure 7(b). In this scenario, energy and exergy efficiencies approximate 23.2% and 24.83%, respectively. Notably, a significant decrease in efficiencies occurs in the combined power plant compared to the combined cycle. The decline is mainly due to significant energy losses in the heliostat field and the receiver, with about 58.52% of the total exergy destruction taking place in the solar field. The overall exergy destruction for the entire plant is calculated to be 45,164 kW, with 37,578 kW attributed solely to the solar field and receiver. The maximum net power output of the combined cycle is 14,930 kW at a CPR of 2.3. Comparison between Figure 7(b) and Figure 7(c) reveals that the inclusion of the TCO_2 cycle into the standalone HBC results in an increased maximum net power output. At the optimal CPR of 2.3, the net power output reaches 14,930 kW for the combined cycle and 13,365 kW for the standalone cycle. This indicates an improvement of 1,565 kW in net power output due to the TCO_2 cycle functioning as the bottoming cycle.

The back work ratio (BWR) is an important system performance metric in addition to efficiency. Better

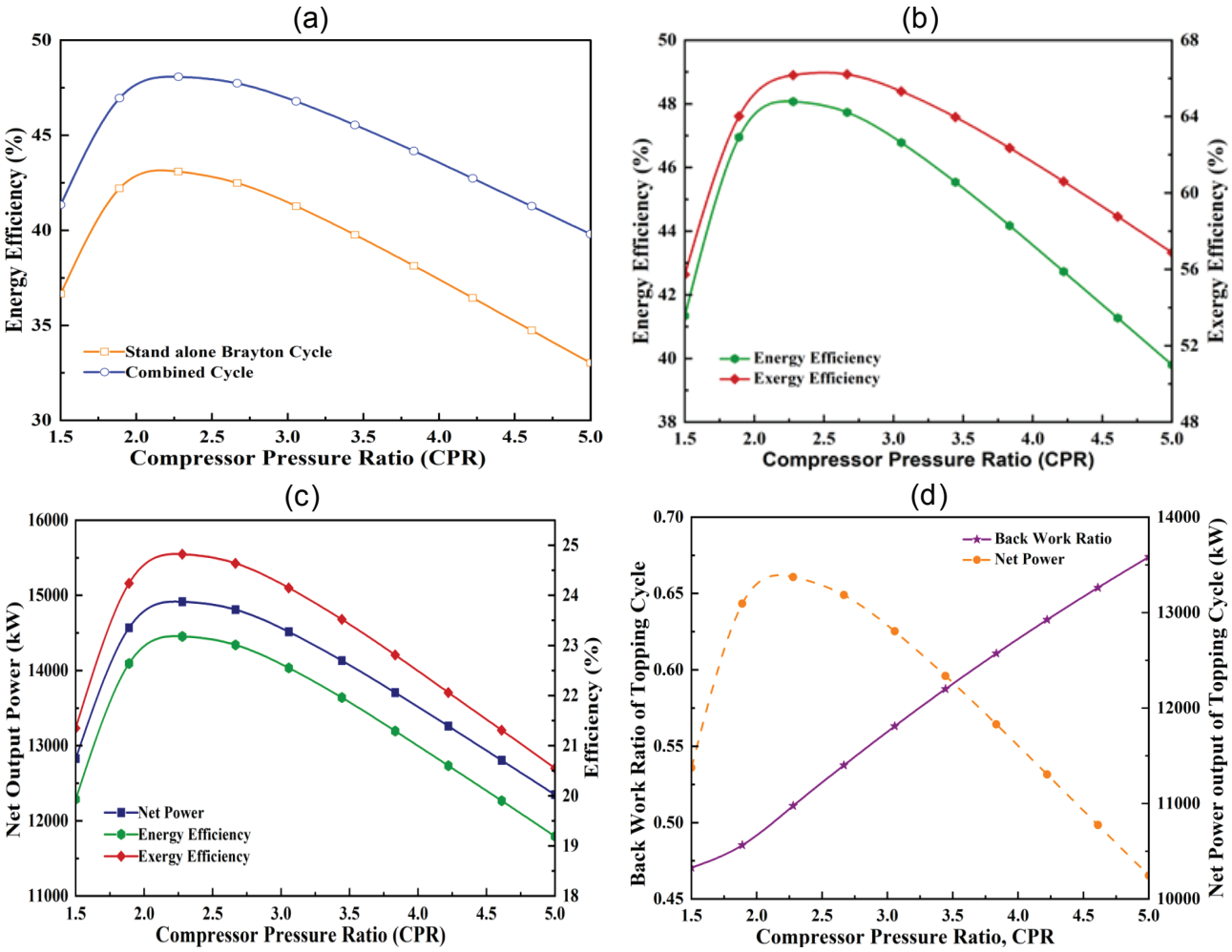

Figure 7. Performance variation with compressor pressure ratio.

overall performance is indicated by a lower BWR, which is the ratio of compressor work to turbine work in a combined cycle. With increasing CPR, BWR also increases, reflecting the continuous rise in compression work, as depicted in Figure 7(d). The connection between BWR and CPR is significant. As CPR increases, the amount of compression work consistently rises, leading to an increase in BWR. The ideal CPR value, however, is found to be 2.3 after taking into account how each other parameter affects system performance. In this case, BWR rises from 0.4712 to 0.6786 while CPR increases from 1.5 to 5. This analysis emphasizes how CPR and BWR interact in a complex way to shape the power cycle's performance characteristics.

Variation in performance with pump pressure ratio

The pump pressure ratio (PPR) has a limited impact on system performance when maintaining a fixed compressor pressure ratio (CPR) of 2.3, a direct normal irradiance (DNI) of 850 W/m², and a helium turbine inlet temperature of 800 °C. The study reveals that the net output power of the TCO_2 cycle and overall plant efficiency experience a continuous increase followed by a decrease as PPR varies. This trend is a result of the influence of PPR on the expansion ratio of the transcritical turbine, where an initial increase in PPR results in higher work output until a critical point is reached at PPR 3.056. After this point, compression work exceeds expansion work, which lowers net work output. As shown in Figure 8(a) for the TCO_2 cycle, the ideal PPR value is 3.056, exhibiting maximum power output, energy efficiency, and exergy efficiency of 1556 kW, 24.83%, and 23.18%, respectively. Additionally, the TCO_2 cycle's BWR reacts to variations in PPR, showing a steady rise with higher PPR values. The net power output first increases and then gradually decreases, as shown in Figure 8(b). As PPR rises from 1.5 to 5, BWR varies from 0.3 to 0.72, with 3.03 being the ideal value. The BWR is 0.49 at this ideal PPR value, meaning that the pump uses 49% of the work output generated by the turbine for compression work.

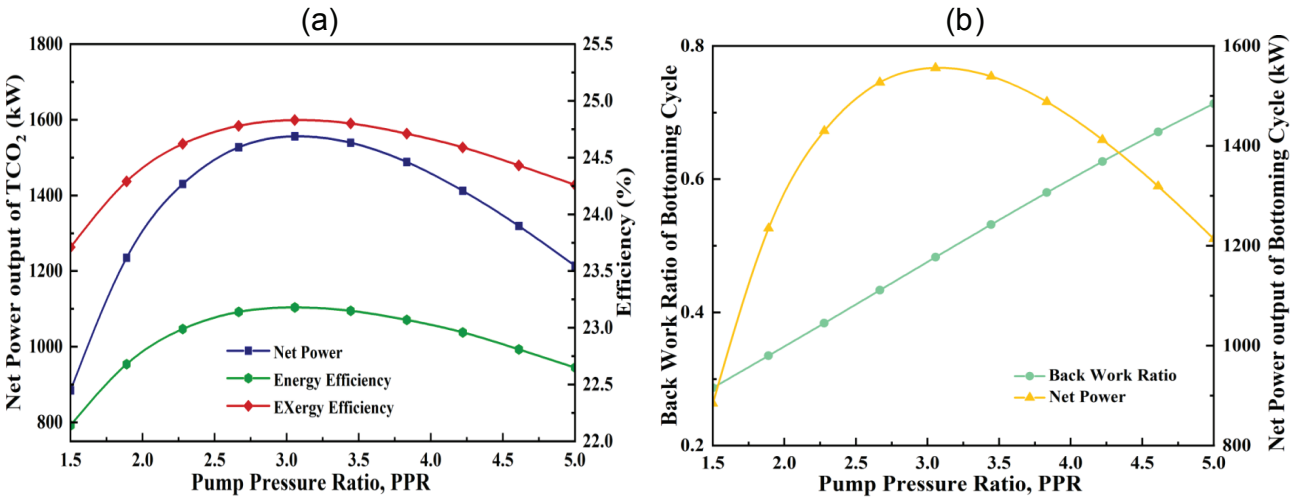

Figure 8. Performance variation with pump pressure ratio.

Effect of Helium Turbine Inlet Temperature

The system's performance is highly dependent on the Helium Turbine Inlet Temperature (HTIT). When HTIT rises from 700 °C to 900 °C, several performance indicators improve significantly. As presented in Figure 9(a), the plant's overall energy efficiency increases from 21.36% to 24.65%, the exergy efficiency grows from 22.87% to 26.4%, and the net power output rises from 13,746 kW to 15,866 kW. At higher HTIT values, the enthalpy difference across the turbine increases, resulting in a greater expansion ratio and this improvement. As a result, the system's thermal performance is improved by increasing the net output power. These results are obtained under the assumptions of an optimal compressor pressure ratio (CPR) of 2.3, a direct normal irradiation (DNI) of 850 W/m², and a TCO_2 turbine inlet temperature of 180 °C. HTIT also affects the mass flow distribution of the working fluids. Figure 9(b) indicates that with increasing HTIT, the mass flow rate of air in the solar power tower (SPT) subsystem increases, while the mass flow rates of both carbon dioxide and helium decrease. The higher air flow rate is linked to the greater quantity of heat delivered from the heliostat field to the receiver. The heated air's outlet temperature rises as a result, which lowers its density and increases the air's mass flow rate. On the other hand, because of the enthalpy variation needed to maintain the same work output, higher topping cycle temperatures lower the flow rates of helium and carbon dioxide. Over the HTIT range of 700 °C to 900 °C, the mass flow rates change from 41.63 kg/s to 59.57 kg/s for air, from 59.69 kg/s to 52.02 kg/s for carbon dioxide, and from 21.92 kg/s to 16.14 kg/s for helium.

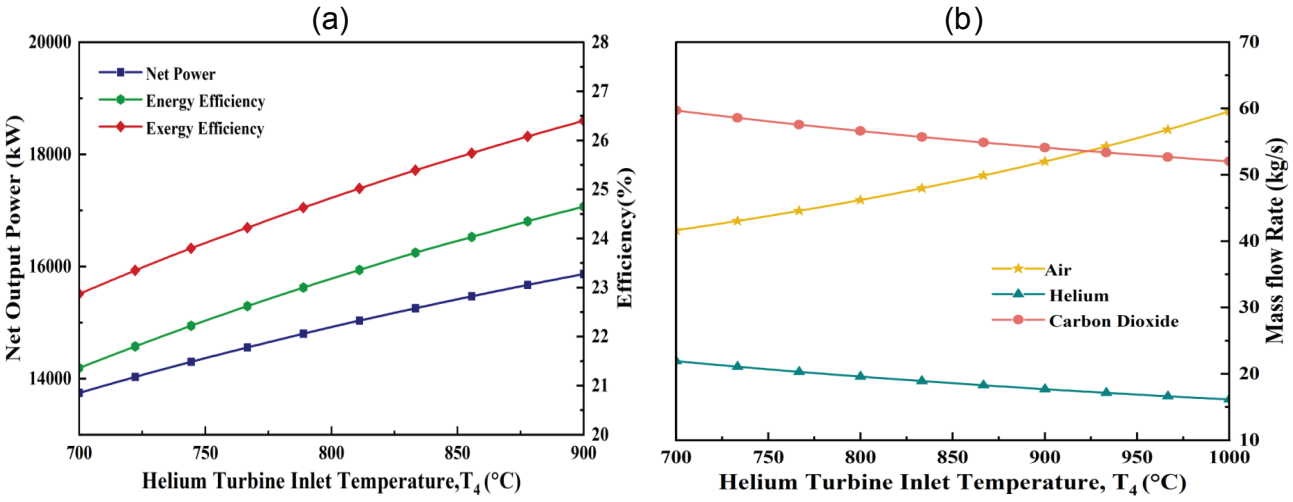

Figure 9. Performance variation with HTIT.

Effect of TCO_2 Turbine Inlet Temperature

This section provides a detailed evaluation of how the TCO_2 turbine inlet temperature influences the overall performance of the system. The overall plant efficiency increases only slightly when the TCO_2 turbine inlet temperature is raised, but the bottoming cycle's net power output responds more strongly. The temperature variation from 150 °C to 200 °C resulted in a modest improvement of 2.05% and 2% in energy and exergy efficiency, respectively. These findings were consistent under constant values of CPR at 2.3, DNI at 850 W/m², and a tCO_2 cycle pump pressure ratio of 3.056, as depicted in Figure 10. In contrast, the net power output of the bottoming cycle exhibited a substantial increase of 22.21%. The temperature increase that results in an increase in thermodynamic properties at the inlet is the cause of this noteworthy phenomenon. As a result, a larger total enthalpy difference developed, which eventually helped to increase the net power output at a fixed pressure ratio.

Impact on system performance of compressor inlet temperature

It is evident how the compressor inlet temperature affects system performance when all other parameters are set as indicated in Table 1. As the compressor's inlet temperature rises, the net power output and overall plant efficiency decrease. This drop, which results from an increasing enthalpy difference across the compressor, has a detrimental effect on the compressor's performance. As a result, the overall system performs worse when the compressor's inlet temperature increases. The energy and energy efficiency of the entire system have decreased from 23.36% to 23% and

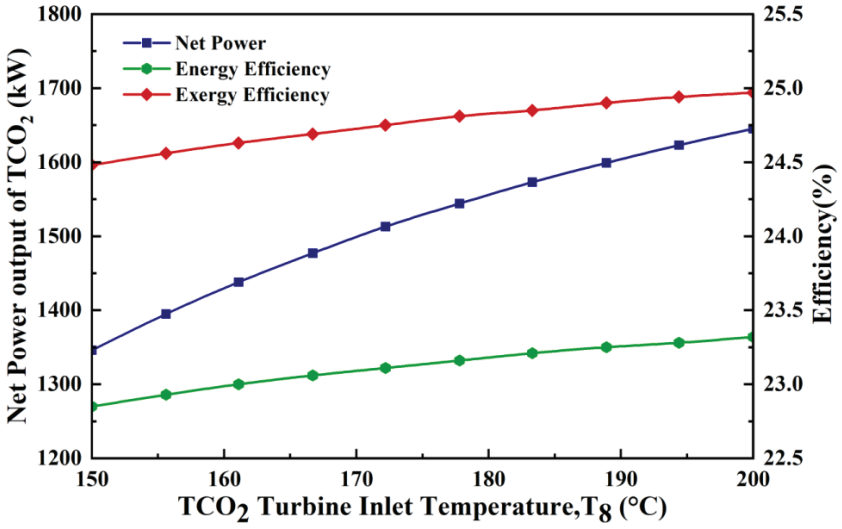

Figure 10. Performance variation of TCO_2 cycle with TCO_2 turbine inlet temperature.

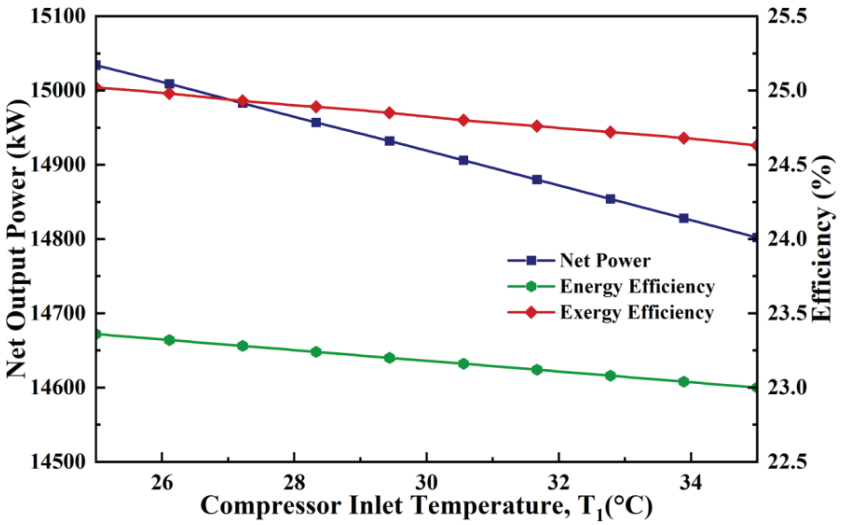

Figure 11. Plant performance variation with compressor inlet temperature.

from 25.02% to 24.63%, respectively. Additionally, Figure 11 shows that power production decreases from 15,034 to 14,802 kW as the temperature rises from 25 to 35 degrees Celsius.

Impact of Solar Subsystem Characteristics on System Performance

Apart from the combined cycle parameters, it is also important to examine how the SPT design parameters affect the power plant. Among them, the efficiency of the heliostat field stands out as the key factor influencing overall performance. A direct correlation is observed: the power plant's total performance improves with an increase in heliostat efficiency. Exergy efficiency, energy efficiency, and power output all experienced significant increases as heliostat efficiency rose from 0.6 to 0.85, as depicted in Figure 12(a). As a result, the energy efficiency increased from 21.64% to 30.65%, the power output increased from 13925 kW to 19728 kW, and the energy efficiency increased from 31.7% to 41.45%. This enhancement can be attributed to the higher heliostat efficiency, which leads to reduced energy loss from the sun and increased energy conversion, consequently boosting exergy, energy, and power output.

The solar intensity, expressed as DNI, stands out as a vital factor with geographical and temporal variability. A distinct relationship that emphasizes the importance of DNI on the power plant's performance metrics is shown in Figure 12(b). It is noteworthy that higher DNI levels are associated with higher system output power, energy efficiency, and exergy efficiency. This relationship stems from the system's capacity to absorb more solar radiation when its DNI is higher, which in turn increases the total amount of heat input. As a result, the mass flow rate of the working fluid increases, leading to a significant rise in work output. For example, when the direct normal irradiation (DNI) changes from 600 to 1000 W/m^2, the work output grows from 10,529 kW to 17,551 kW. Simultaneously, energy and exergy efficiencies exhibit a steady increase from 16.36% to 27.3% and 17.52% to 29.4%, respectively.

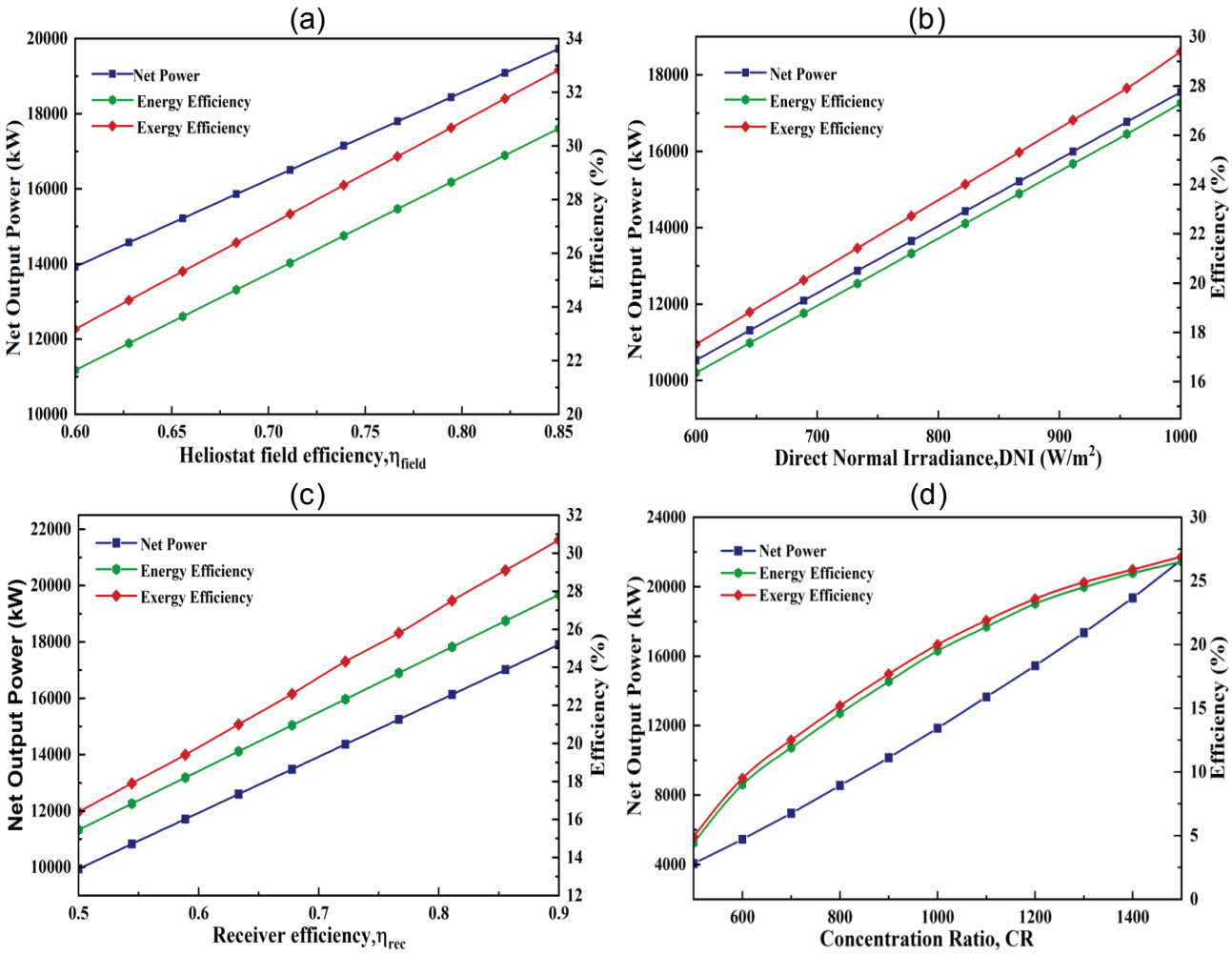

Figure 12. Plant performance variation with heliostat field efficiency.

The overall performance of the system is greatly influenced by the efficiency of the receiver, as shown in Figure 12(c). The overall performance of the system improves as the receiver efficiency () rises. This improvement is explained by the fact that higher receiver efficiency results in less heat loss, which allows the system to produce a significant amount more heat. Figure 12(c) shows a clear trend, where an increase in receiver efficiency from 0.5 to 0.9 raises the work output from 9,946 kW to 17,903 kW. Simultaneously, energy and exergy efficiencies show a steady ascent from 15.45% to 27.82% and 16.39% to 30.7%, respectively. The concentration ratio, which varies between 300 and 1500 in solar power tower plants, is another key factor affecting power plant performance, as illustrated in Figure 12(d). With a fixed heliostat area (A_{hel}), an elevation in the concentration ratio results in a reduction in the aperture area of the receiver. This, in turn, leads to a higher solar heat flux into the receiver, contributing to an increase in both the plant's net power production and efficiency. Figure 12(d) highlights this correlation, emphasizing that efficiency improvements are more significant at lower concentration ratios. However, the potential for improving energy and exergy efficiency decreases as the concentration ratio increases, mainly because of increased exergy destruction.

Effects of Various Parameters on Exergoenvironmental Performance

Exergoenvironmental analysis is an approach used in the study of thermodynamics and sustainability to evaluate and examine how energy systems and processes affect the environment. Figure 13(a) depicts the effect of the compressor pressure ratio on exergoenvironmental factors. It is evident from the figure that, as CPR increases, the environmental impact index (θ_{ei}) decreases and reaches a minimum value of 3 at a pressure ratio of 2.3. Subsequently, it gradually increases with further pressure ratio increments. This phenomenon arises due to lower exergy destruction at lower pressure ratios, which becomes more pronounced at higher pressure ratios. Similarly, other environmental factors such as the environmental impact factor (θ_{eii}), exergy sustainability index (θ_{est}), and exergy stability factor (f_{es})

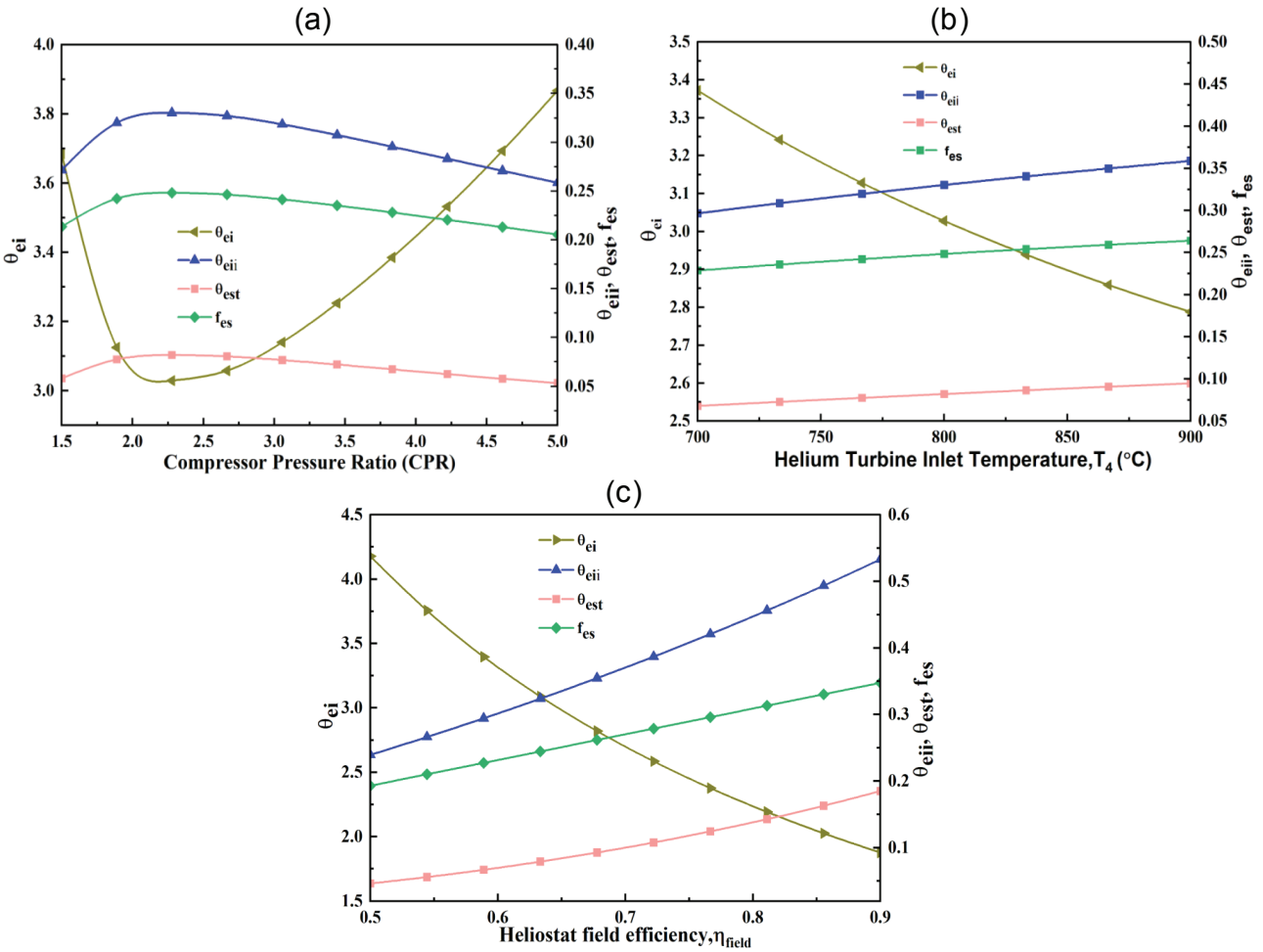

Figure 13. Exergoenvironmental factors variation with various parameters.

exhibit a similar trend. Exergy efficiency increases with a pressure ratio up to 2.3 and then declines as the pressure ratio continues to rise. In the graph, θ_{ei} decreases from 3.68 to 3 at a CPR of 2.33 and then increases to 3.8 at a CPR of 5. The factors θ_{eii}, θ_{est}, and f_{es} increases from 0.27 to 0.32, 0.05 to 0.07, and 0.21 to 0.24, respectively, as CPR increases from 1.5 to 2.33, reaching their optimum values at 2.3 and subsequently decreasing with further pressure ratio increases.

Figure 13(b) illustrates the effect of helium turbine inlet temperature on exergoenvironmental factors. It can be observed that, as the turbine inlet temperature of the HBC increases, θ_{ei} decreases, whereas the other factors, namely θ_{eii}, θ_{est}, and f_{es}, increases with the rising turbine inlet temperature. This trend is a result of the minimum exergy destruction at lower temperatures, while higher temperatures lead to increased exergy destruction. The θ_{ei} decreases from 3.37 to 2.78, while the factors θ_{eii}, θ_{est}, and f_{es} increases from 0.29 to 0.35, 0.06 to 0.09, and 0.2 to 0.26, respectively, as the temperature rises from 700 °C to 900 °C.

Figure 13 (c) illustrates the relationship between heliostat field efficiency and exergoenvironmental factors. As observed in the graph, θ_{ei} decreases, while the other factors, including θ_{eii}, θ_{est} and f_{es}, increase as heliostat field efficiency rises from 50% to 90%. The value of θ_{ei} decreases from 4.17 to 1.8, while the factors θ_{eii}, θ_{est}, and f_{es} increases from 0.23 to 0.53, 0.04 to 0.18, and 0.19 to 0.34, respectively. This trend emerges because the heliostat field receives the maximum amount of solar energy, with temperatures around 2000 °C. Consequently, such high temperatures result in maximum exergy destruction within the heliostat field. Therefore, it can be concluded that the present study has a negligible harmful impact on the environment, and thus power is generated in a carbon free manner.

Comparison With Previous Research

The present system comprises a helium Brayton cycle, a waste heat recovery transcritical CO_2 (TCO_2) cycle serving as the bottoming cycle, and a solar power tower (SPT) system. This system has been compared to previous studies by Zare and Hasanzadeh [17]. It is clear that the current system (energy efficiency 23.2%) may attain almost the same thermal performance as the Zare and Hasanzadeh [17] system (energy efficiency 23.11%) with fewer components. While the current study only included 11 components for the same thermal efficiency for the high-temperature SPT applications, Zare and Hasanzadeh [17] included 17 components.

CONCLUSION

This study proposes an integrated hybrid Brayton cycle (HBC) and transcritical CO_2 (TCO_2) cycle for harnessing solar energy from the solar power tower (SPT) system to improve the overall plant performance. The exergy, energy and exergoenvironmental analysis have been performed to analyze the performance using the EES software. Further, following conclusions were made from the results and discussion section;

- Incorporating the transcritical CO_2 (TCO_2) cycle as a bottoming cycle to the standalone hybrid Brayton cycle (HBC) resulted in a 12.05% improvement.
- The SPT subsystem (receiver and heliostats) accounted for the highest exergy destruction rate, comprising approximately 83.20% of the exergy destruction (total 45,164 kW) in the entire plant.
- According to the parametric analysis, net output power, overall plant energy and exergy efficiency, and CPR first increased before declining. The highest values 23.2%, 24.84%, and 14930 kW, respectively—were attained at an ideal CPR of 2.3. The overall performance of the plant is not significantly impacted by TCO_2 cycle parameters like PPR and TCO_2 turbine inlet temperature.
- The exergoenvironmental impact coefficient, with a high value of 4.028, reflects the lower exergy efficiency of the plant and suggests substantial potential for reducing environmental effects.
- The exergetic stability factor was determined to be 0.2483, which is close to the preferable value of one for a power-generating plant.
- This analysis offers the potential of developing a highly efficient power system for future carbon-free power generation with less complexity as compared to previous research.
- The exergoeconomic analysis of this resent work need to be performed in future study.
- This study is confined to peak load conditions owing to the absence of a solar energy storage system.

NOMENCLATURE

A	Area (m^2)
$\dot{E}X$	Rate of exergy (kW)
$\dot{E}D$	Exergy destruction rate (kW)
N_{hel}	Number of heliostats
$\dot{Q}$	Rate of heat interaction (kW)
$\dot{m}$	Mass flow rate (kg/s)
h	Specific enthalpy (kJ/kg)
T	Temperature (K)
s	Specific entropy (kJ/kg·K)
$\dot{W}$	Power (kW)

Abbreviations

WHRU	Waste heat recovery unit
COND	Condenser
TCO_2	Transcritical CO_2
sCO_2	Supercritical CO_2
SPT	Solar power tower
PPR	Pump pressure ratio
ORC	Organic Rankine cycle
HBC	Helium Brayton cycle
HT	Helium turbine
DNI	Direct normal irradiation (W/m^2)

HC Helium compressor
CPR Compressor pressure ratio
IHE Intermediate heat exchanger

Subscripts
e exit
i inlet
rec receiver
0 dead condition
j particular state
hel heliostat
ref reference/reflectivity

Greek letters
η Efficiency
ε Effectiveness

AUTHORSHIP CONTRIBUTIONS

Authors equally contributed to this work.

DATA AVAILABILITY STATEMENT

The authors confirm that the data that supports the findings of this study are available within the article. Raw data that support the finding of this study are available from the corresponding author, upon reasonable request.

CONFLICT OF INTEREST

The author declared no potential conflicts of interest with respect to the research, authorship, and/or publication of this article.

ETHICS

There are no ethical issues with the publication of this manuscript.

STATEMENT ON THE USE OF ARTIFICIAL INTELLIGENCE

Artificial intelligence was not used in the preparation of the article

REFERENCES

[1] IEA. Electricity 2024. Available at: https://www.iea.org/reports/electricity-2024. Accessed on Dec 25, 2025.

[2] Khan Y, Raman R, Rashidi MM, et al. Thermodynamic analysis, and experimental investigation of the water spray cooling of photovoltaic solar panels. J Therm Anal Calorim 2023;148:5591–5602. [Crossref]

[3] Khan Y, Singh D, Sharma S, Gupta S, Joshi SK, Tevatia A. Comprehensive analysis of a high temperature solar powered trigeneration system: An energy, exergy, and exergo-environmental (3E) assessment. Proceedings of the Institution of Mechanical Engineers, Part C: J Mech Eng Sci 2024;238(16):8446-8463. [Crossref]

[4] Khan Y, Singh D, Kumar S, Mishra S, Anjum A, Asdaque PMG. Performance evaluation of the combined helium Brayton cycle and organic Rankine cycles for solar power tower application A comparative study. J Renew Sustain Energy 2024;16(6). [Crossref]

[5] Khan Y, Mishra RS. Parametric (exergy-energy) analysis of parabolic trough solar collector-driven combined partial heating supercritical CO2 cycle and organic Rankine cycle. Energy sources, part A: recovery, utilization, and environmental effects 2020;1-27. [Crossref]

[6] Kumar KS, Razak A, Yadav A, Rao PR, Majdi HS, Khan TY, Singh K. Experimental analysis of cycle tire pyrolysis oil doped with 1-decanol+ TiO2 additives in compression ignition engine using RSM optimization and machine learning approach. Case Stud Therm Eng 2024;61:104863. [Crossref]

[7] Khandelwal N, Sharma M, Singh O, Shukla AK. Recent developments in integrated solar combined cycle power plants. J Therm Sci 2020;29(2):298-322. [Crossref]

[8] Chauhan MK, Chauhan AK, Khan Y, Singh AP. Experimental and theoretical investigation of thermal efficiency and productivity of single slope basin type solar distillation system using honey-comb. J Ther Eng 2023;9(6):1559−1571. [Crossref]

[9] Khan Y, Tevatia A, Apparao D, Singh N, Mishra S. Experimental investigation to evaluate thermal performance of a solar cooker with evacuated tube solar collector using different heat transfer fluids. J Ther Eng 2024;10(5):1335−1346. [Crossref]

[10] Farabi SN, Habib K, Mim M, Zaed MA, Ali SA, Younas M, Saidur R. The future of solar-driven interfacial steam generation for sustainable water desalination: drivers, challenges, and opportunities-Review. Results Eng 2024;102649. [Crossref]

[11] Shukla AK, Sharma A, Sharma M, Nandan G. Thermodynamic investigation of solar energy-based triple combined power cycle. Energy Sources, Part A: Recovery, Utilization, and Environmental Effects 2019;41(10):1161-1179. [Crossref]

[12] Khan Y, Singh D, Caliskan H, et al. Exergoeconomic and Thermodynamic Analyses of Solar Power Tower Based Novel Combined Helium Brayton Cycle-Transcritical CO2 Cycle for Carbon Free Power Generation. Global Challenges 2023; 7: 2300191. [Crossref]

[13] Islam MT, Huda N, Abdullah AB, Saidur R. A comprehensive review of state-of-the-art concentrating solar power (CSP) technologies: Current status and research trends. Renew Sustain Energy Rev 2019;91:987-1018. [Crossref]

[14] Khan Y, Mishra RS. Thermo-economic analysis of the combined solar based pre-compression supercritical CO2 cycle and organic Rankine cycle using ultra-low GWP fluids. Therm Sci Eng Prog 2021;23: 100925. [Crossref]
[15] Sachdeva J, Singh O. Thermodynamic analysis of solar powered triple combined Brayton, Rankine, and organic Rankine cycle for carbon free power. Renew Energy 2019;139:765-780. [Crossref]
[16] Fan G, Song J, Zhang J, Fu Z, Gong X, Dai Y, Markides CN. Thermo-economic assessment and systematic comparison of combined supercritical CO2 and organic Rankine cycle (SCO2-ORC) systems for solar power tower plants. Appl Therm Eng 2024;236:121715. [Crossref]
[17] Khan Y, Mishra RS. Performance analysis of a solar-based novel trigeneration system using cascaded vapor absorption-compression refrigeration system, Int J Refrig 2023. [Crossref]
[18] Habibi H, Zoghi M, Chitsaz A, Javaherdeh K, Ayazpour M, Bellos E. Working fluid selection for regenerative supercritical Brayton cycle combined with bottoming ORC driven by molten salt solar power tower using energy–exergy analysis. Sustain Energy Technol and Assess 2020;39:100699. [Crossref]
[19] Liu Y, Wang Y, Huang D. Supercritical CO2 Brayton cycle: A state-of-the-art review. Energy 2019;189:115900. [Crossref]
[20] Ehsan MM, Awais M, Lee S, Salehin S, Guan Z, Gurgenci H. Potential prospects of supercritical CO2 power cycles for commercialisation: Applicability, research status, and advancement. Renew Sustain Energy Rev 2023;172:113044. [Crossref]
[21] Li MJ, Zhu HH, Guo JQ, Wang K, Tao WQ. The development technology and applications of supercritical CO2 power cycle in nuclear energy, solar energy and other energy industries. Appl Therm Eng 2017;126:255-275. [Crossref]
[22] Gkountas AA, Benos LT, Nikas KS, Sarris IE. Heat transfer improvement by an Al2O3-water nanofluid coolant in printed-circuit heat exchangers of supercritical CO2 Brayton cycle. Therm Sci Eng Prog 2020;20:100694. [Crossref]
[23] Chai L, Tassou SA. Influence of Operation Parameters on Thermohydraulic Performance of Supercritical CO2 in a Printed Circuit Heat Exchanger. Heat Transf Eng 2024;1-19. [Crossref]
[24] Al-Sulaiman FA, Atif M. Performance comparison of different supercritical carbon dioxide Brayton cycles integrated with a solar power tower. Energy 2015;82:61-71. [Crossref]
[25] Atif M, Al-Sulaiman FA. Optimization of heliostat field layout in solar central receiver systems on annual basis using differential evolution algorithm. Energy Convers Manage 2015;95:1-9. [Crossref]
[26] Javanshir A, Sarunac N, Razzaghpanah Z. Thermodynamic analysis of simple and regenerative Brayton cycles for the concentrated solar power applications. Energy Convers Manage *2018;*163:428-443. [Crossref]
[27] Hashemian N, Noorpoor A. Assessment and multi-criteria optimization of a solar and biomass-based multi-generation system: Thermodynamic, exergoeconomic and exergoenvironmental aspects. Energy Convers Manage 2019;195:788-797. [Crossref]
[28] Zainul R, Basem A, Alfaker MJ, Sharma P, Kumar A, Al-Bahrani M, Pandey S. Exergy, exergoeconomic optimization and exergoenvironmental analysis of a hybrid solar, wind, and marine energy power system: A strategy for carbon-free electrical production. Heliyon 2024;10(16). [Crossref]
[29] Yang K, He Y, Du N, Yan P, Zhu N, Chen Y, Lund PD. Exergy, exergoeconomic, and exergoenvironmental analyses of novel solar-and biomass-driven trigeneration system integrated with organic Rankine cycle. Energy 2024;301: 131605. [Crossref]
[30] Rahimimotlagh Z, Ahmadi A. Energy, exergy, exergoeconomic and exergoenvironmental analysis and optimization of combined solar, SRC cycles with compressed air energy storage (CAES) and methane production system. Energy Convers Manage 2024;317:118855. [Crossref]
[31] Qi X, Yang C, Huang M, Ma Z, Hnydiuk-Stefan A, Feng K, Li Z. Conventional and advanced exergy-exergoeconomic-exergoenvironmental analyses of an organic Rankine cycle integrated with solar and biomass energy sources. Energy 2024;288:129657. [Crossref]
[32] Zhou F, Zhu L, Fu W, Sardari F. Thermodynamic and exergoenvironmental analysis of a new solar-driven cogeneration system integrated with a solar still desalination unit. Appl Therm Eng 2023;234:121241. [Crossref]
[33] Cavalcanti EJC. Exergoeconomic and exergoenvironmental analyses of an integrated solar combined cycle system. Renew Sustain Energy Rev 2019;67:507-519. [Crossref]
[34] Su Z, Yang L, Wang H, Song J, Jiang W. Exergoenvironmental optimization and thermoeconomic assessment of an innovative multistage Brayton cycle with dual expansion and cooling for ultra-high temperature solar power. Energy 2024;286:129581. [Crossref]
[35] Guo JQ, Li MJ, Xu JL, Yan JJ, Wang K. Thermodynamic performance analysis of different supercritical Brayton cycles using CO2-based binary mixtures in the molten salt solar power tower systems. Energy 2019;173:785-798. [Crossref]
[36] Trevisan S, Guédez R, Laumert B. Thermo-economic optimization of an air driven supercritical CO2 Brayton power cycle for concentrating solar power plant with packed bed thermal energy storage. Solar Energy 2020;211: 1373-1391. [Crossref]

[37] Niu X, Ma N, Bu Z, Hong W, Li H. Thermodynamic analysis of supercritical Brayton cycles using CO2-based binary mixtures for solar power tower system application. Energy 2022;254:124286. [Crossref]
[38] Wan X, Wang K, Zhang CM, Zhang TC, Min CH. Off-design optimization for solar power plant coupling with a recompression supercritical CO2 Brayton cycle and a turbine-driven main compressor. Appl Therm Eng 2022;209:118281. [Crossref]
[39] Lu Q, Zhao J, Fang S, Ye W, Pan S. Investigation of thermodynamics of the supercritical CO2 Brayton cycle used in solar power at off-design conditions. Sustain Energy Technol Assess 2022;52:102361. [Crossref]
[40] Bai W, Li H, Zhang X, Qiao Y, Zhang C, Gao W, Yao M. Thermodynamic analysis of CO2–SF6 mixture working fluid supercritical Brayton cycle used for solar power plants. Energy 2022;261:124780. [Crossref]
[41] Ma YN, Hu P, Jia CQ, Wu ZR, Chen Q. Thermo-economic analysis and multi-objective optimization of supercritical Brayton cycles with CO2-based mixtures. Appl Therm Eng 2023;219:119492. [Crossref]
[42] Khademi M, Ahmadi A, Dashti R, Shirmohammadi R. Thermoeconomic optimization of a solar-assisted supercritical CO2 Brayton cycle, organic Rankine cycle and multi-effect distillation system. Energy Rep 2022;8: 13494-13503. [Crossref]
[43] Liu Y, Wang Y, Zhang Y, Hu S. Design and performance analysis of compressed CO2 energy storage of a solar power tower generation system based on the S-CO2 Brayton cycle. Energy Convers Manage 2021;249: 114856. [Crossref]
[44] Goyal A, Sherwani AF. Optimization of exergetic performance and payback period of organic rankine cycle integrated vapor compression refrigeration system based on exergy, economic, and environmental criteria. J Ther Eng 2023;9(3):648-658. [Crossref]
[45] Khan Y, Mishra RS, Raman R, Hashmi AW. Parametric evaluation of solar integrated combined partial cooling supercritical CO2 cycle and Organic Rankine Cycle using low global warming potential fluids. J Ther Eng 2023;9(5):1140−1152. [Crossref]
[46] Cao Y, Dhahad HA, Togun H, Anqi AE, Farouk N, Farhang B. Proposal and thermo-economic optimization of using LNG cold exergy for compressor inlet cooling in an integrated biomass fueled triple combined power cycle. Int J Hydrogen Energy 2021;46(29):15351-15366. [Crossref]
[47] Olumayegun O, Wang M, Kelsall G. Closed-cycle gas turbine for power generation: A state-of-the-art review. Fuel 2016;180:694-717. [Crossref]
[48] Khatoon S, Kim MH. Performance analysis of carbon dioxide based combined power cycle for concentrating solar power. Energy Convers Manage 2020;205:112416. [Crossref]
[49] Dezfouli AHM, Niroozadeh N, Jahangiri A. Energy, exergy, and exergoeconomic analysis and multi-objective optimization of a novel geothermal driven power generation system of combined transcritical CO2 and C5H12 ORCs coupled with LNG stream injection. Energy 2023;262:125316. [Crossref]
[50] Abdollahpour A, Ghasempour R, Kasaeian A, Ahmadi MH. Exergoeconomic analysis and optimization of a transcritical CO2 power cycle driven by solar energy based on nanofluid with liquefied natural gas as its heat sink. J Therm Anal Calorim 2020;139(1):451-473. [Crossref]
[51] Meng N, Li T, Kong X, Gao X. Advanced exergy and exergoeconomic analyses and a case study of a novel trans-critical CO2 cycle with pressurization process for hot dry rock. Energy Convers Manage 2021;246: 114687. [Crossref]
[52] Khan Y, Mishra RS, Singh AP. Performance comparison of organic Rankine cycles integrated with solar based combined cycle: A thermodynamic and exergoenvironmental analysis. Proc Inst Mech Eng Pt C J Mechan Eng Sci 2024;238(1):233-248. [Crossref]
[53] Khan Y, Raman R, Rashidi MM, Said Z, Caliskan H, Hoang AT. Thermodynamic and exergoenvironmental assessments of solar-assisted combined power cycle using eco-friendly fluids. J Therm Anal Calorim 2024;149(3):1125-1139. [Crossref]